AD

TECHNICAL REPORT ARCCB-TR-97011

EROSION MODELING OF THE 120-MM M256/M829A2 GUN SYSTEM

SAMUEL SOPOK
PETER O'HARA
PATRICK VOTTIS
GEORGE PFLEGL
CHRISTOPHER RICKARD
RICHARD LOOMIS

19970603 094

APRIL 1997

US ARMY ARMAMENT RESEARCH, DEVELOPMENT AND ENGINEERING CENTER
CLOSE COMBAT ARMAMENTS CENTER
BENÉT LABORATORIES
WATERVLIET, N.Y. 12189-4050

APPROVED FOR PUBLIC RELEASE; DISTRIBUTION UNLIMITED

DTIC QUALITY INSPECTED 3

DISCLAIMER

The findings in this report are not to be construed as an official Department of the Army position unless so designated by other authorized documents.

The use of trade name(s) and/or manufacturer(s) does not constitute an official indorsement or approval.

DESTRUCTION NOTICE

For classified documents, follow the procedures in DoD 5200.22-M, Industrial Security Manual, Section II-19 or DoD 5200.1-R, Information Security Program Regulation, Chapter IX.

For unclassified, limited documents, destroy by any method that will prevent disclosure of contents or reconstruction of the document.

For unclassified, unlimited documents, destroy when the report is no longer needed. Do not return it to the originator.

REPORT DOCUMENTATION PAGE

Form Approved
OMB No. 0704-0188

Public reporting burden for this collection of information is estimated to average 1 hour per response, including the time for reviewing instructions, searching existing data sources, gathering and maintaining the data needed, and completing and reviewing the collection of information. Send comments regarding this burden estimate or any other aspects of this collection of information, including suggestions for reducing this burden, to Washington Headquarters Services, Directorate for Information Operations and Reports, 1215 Jefferson Davis Highway, Suite 1204, Arlington, VA 22202-4302, and to the Office of Management and Budget, Paperwork Reduction Project (0704-0188), Washington, DC 20503.

1. AGENCY USE ONLY (Leave blank)	2. REPORT DATE	3. REPORT TYPE AND DATES COVERED
	April 1997	Final

4. TITLE AND SUBTITLE
EROSION MODELING OF THE
120-MM M256/M829A2 GUN SYSTEM

5. FUNDING NUMBERS
AMCMS No. 6226.24.H180.0
PRON No. 4A7A7FYK1ABJ

6. AUTHOR(S)
Samuel Sopok, Peter O'Hara, Patrick Vottis, George Pflegl,
Christopher Rickard, and Richard Loomis (PM-TMAS, Dover, NJ)

7. PERFORMING ORGANIZATION NAME(S) AND ADDRESS(ES)
U.S. Army ARDEC
Benet Laboratories, AMSTA-AR-CCB-O
Watervliet, NY 12189-4050

8. PERFORMING ORGANIZATION REPORT NUMBER
ARCCB-TR-97011

9. SPONSORING/MONITORING AGENCY NAME(S) AND ADDRESS(ES)
U.S. Army ARDEC
Close Combat Armaments Center
Picatinny Arsenal, NJ 07806-5000

10. SPONSORING/MONITORING AGENCY REPORT NUMBER

11. SUPPLEMENTARY NOTES
Presented at the 1997 ADPA Gun and Ammunition Symposium, San Diego, CA, 7-10 April 1997.
Published in proceedings of the conference.

12a. DISTRIBUTION/AVAILABILITY STATEMENT
Approved for public release; distribution unlimited.

12b. DISTRIBUTION CODE

13. ABSTRACT (Maximum 200 words)

The Benet Laboratories/Software and Engineering Associates, Inc. (SEA) gun barrel erosion modeling and design code predicts wall degradation due to transformations, chemical reactions, and cracking coupled with pure mechanical erosion for the 120-mm M256/M829A2 gun system for ambient temperature-conditioned rounds. The A723 steel and 0.005-inch high contraction (HC) chromium plated/A723 steel wall materials are evaluated for erosion. This complex computer analysis is based on rigorously evaluated scientific theory that has been validated in the rocket community over the last forty years. Our gun erosion analysis includes the standard interior ballistics gun code (XNOVAKTC), the standard nonideal gas-wall thermochemical rocket code modified for guns (CCET), the standard mass addition boundary layer rocket code modified for guns (MABL), and the standard wall material ablation conduction erosion rocket code modified for guns (MACE). In addition, bore subsurface metallographic analysis and projectile-bore finite element analysis (ABAQUS) are considered. Our overall analysis provides wall material erosion predictions and comparisons of ablation, conduction, and erosion profiles as a function of time, travel (customer-selected 27, 61, 86, 130, and 201 inches from the rear face of the tube), and number of rounds to barrel condemnation. The 120-mm M256/M829A2 gun system prediction, with significant numbers of M829A2 rounds, agrees well with the wear and erosion pattern of retired M256 gun barrels.

14. SUBJECT TERMS
Erosion Modeling, 120-mm M256/M829A2 Gun System,
Gun Barrels, Chromium, Steel

15. NUMBER OF PAGES
24

16. PRICE CODE

17. SECURITY CLASSIFICATION OF REPORT	18. SECURITY CLASSIFICATION OF THIS PAGE	19. SECURITY CLASSIFICATION OF ABSTRACT	20. LIMITATION OF ABSTRACT
UNCLASSIFIED	UNCLASSIFIED	UNCLASSIFIED	UL

TABLE OF CONTENTS

Page

INTRODUCTION 1

THEORY AND PROCEDURE 1

RESULTS AND DISCUSSION 3

REFERENCES 9

LIST OF ILLUSTRATIONS

1. Gun Erosion Modeling Overview 11

2. Ambient-Conditioned M829A2 XNOVAKTC Gas Pressures 12

3. Ambient-Conditioned M829A2 XNOVAKTC Gas Temperatures 13

4. Ambient-Conditioned M829A2 XNOVAKTC Gas Velocities 14

5. Ambient-Conditioned M829A2 MABL Recovery Enthalpies 15

6. Ambient-Conditioned M829A2 MABL Cold Wall Heat Flux 16

7. M829A2 CCET Reacting Wall Enthalpies 17

8. M829A2 CCET Ablation and Melting Potential 18

9. M829A2 27" RFT Inhibited Growth Fit of Subsurface Exposure Test Data 19

10. M829A2 Typical Relative Rounds-to-Plate Spalling Based on Subsurface Exposure and Flow Modeling at 27" RFT 20

11. MACE Ambient-Conditioned M829A2 Maximum Wall and Interface Temperatures 21

12. MACE Ambient-Conditioned M829A2 Cumulative Wall Erosion-to-Condemnation 22

13. 120-mm M256/M829A2 Erosion Modeling Concurs with the Typical Wear and Erosion Pattern of Retired M256 Gun Barrels with M829A2 Rounds 23

INTRODUCTION

The study of chemical reactions in flow systems (aerothermochemistry) was first described by von Karman in 1951 (ref 1). The modification of the heat transfer coefficient (blocking) for the mass addition of chemically reacting wall material into the boundary layer was first described by Reshotko and Cohen in 1955 (refs 2,3). The thermochemical erosion of reentry vehicle heat shield material for various chemically reacting systems was first studied by Denison and Dooley in 1957 (ref 4). This thermochemical erosion theory was unified and summarized by Lees of CalTech and The Ramo-Wooldridge Corporation in 1958 (ref 5). The near exclusive use of Lees' now JANNAF standardized model (refs 6-8) has stood the test of time and demonstrates that the major assumptions are still reasonable and valid.

Gun barrel technology has focused on reducing mechanical and metallurgical gun barrel failures with great success, while gun barrel thermochemical erosion has intensified due to performance requirements demanding the use of high-flame temperature propellants. Many ADPA Tri-Service sponsored gun erosion meetings have implied a thermochemical erosion mechanism for various gun systems, and U.S. Army experimental data support the existence of gun barrel oxidation (refs 9,10). Practical gun barrel design should protect against the lower temperature thermochemical erosion and remain below the higher temperature thermal erosion.

In 1992, after an exhaustive search, U.S. Army Benet Laboratories (Benet) teamed with Software and Engineering Associates (SEA) to successfully modify their JANNAF standard rocket erosion codes (TDK/MACE) (refs 6-8) into the first-known gun barrel erosion modeling code that addresses wall degradation due to thermal (transformations), thermochemical (reactions), and thermomechanical (cracking) effects coupled with pure mechanical erosion (high-speed flow, wear). SEA is the sole maintainer and developer of these rocket erosion codes. The resulting compressible chemical equilibrium and transport (CCET) thermochemistry gun code is much more extensive and robust than the nonideal gas thermochemical equilibrium (BLAKE) code (ref 11). The gun erosion analysis uses standard interior ballistics gun code (XNOVAKTC) (ref 12) core flow data as input. In July 1995, Benet and SEA jointly published (AIAA) the first-known paper describing a gun barrel erosion modeling code (ref 13).

THEORY AND PROCEDURE

This 120-mm M256/M829A2 gun system erosion analysis includes the following codes:

- Standard interior ballistics gun code (XNOVAKTC for core flow) (ref 12)
- Standard nonideal gas-wall thermochemical rocket code modified for guns (CCET for gas-wall transport/chemistry (refs 6,8,13)

- Standard heat transfer modified by mass addition to boundary layer rocket code modified for guns (MABL for transport and cold/adiabatic wall properties (refs 6,13)

- Standard wall material ablation conduction erosion rocket code modified for guns (MACE) (refs 7,13).

In addition, bore subsurface metallographic analysis and ABAQUS projectile-bore finite element analysis (ref 14) are used.

The CCET code (refs 6,8,13) outputs gun system inert/reacting gas-wall enthalpy (H_{gw}), condensed phase products mass fraction (C_{cg}), and ablation potential (B_a) data as a function of pressure and temperature. Combustion product omissions and gas-wall reactivity are based on Benet/SEA experimental testing and U.S. Army reports (ref 10). The CCET code assumes that as the gas diffuses to the wall, it reacts to form products as follows:

$$B_a = (C_w - C_{cg})/C_g \tag{1}$$

where C_w is the mass fraction of wall material and C_g is the mass fraction of the gas edge.

The MABL code (refs 6.13) outputs adiabatic wall recovery enthalpy (H_r) and adiabatic wall temperature (T_{aw}) data as a function of time and travel. The recovery enthalpy is the potential chemistry driver where the heat transfer approaches zero and the adiabatic wall temperature is the potential temperature without reactions. The MABL code also outputs cold wall heat transfer rate (Q_{cw}) data as a function of time and travel. This heat transfer rate is the wall heat flux evaluated at the cold wall temperature. The MABL code heat and mass transfer model includes the following three equations. The first equation is for mass addition to the boundary layer, the second equation is for heat-to-mass transfer ratio, and the third equation is for the overall correlation between the first and second equations:

$$r_e\, U_e\, Ch_o = Q_{cw}/(H_r - H_{gw}) \tag{2}$$

$$r_e\, U_e\, Ch_b = Mdot_g/B_a;\ Le = 1 \tag{3}$$

$$Ch_b/Ch_o = f(B_a, M_w) = 1 - (h\, Mdot_g/r_e\, U_e\, Ch_o) \tag{4}$$

where r_e is edge density, U_e is edge velocity, Ch_o is Stanton number without blowing, Q_{cw} is cold wall heat transfer, H_r is recovery enthalpy, H_{gw} is gas-wall enthalpy, Ch_b is Stanton number with blowing, $Mdot_g$ is gas mass transfer, Le is the Lewis number, B_a is ablation potential, M_w is molecular weight, and h is a function of g-BL molecular diffusion.

The MACE code (refs 7,13) calculates the actual transient thermochemical response and generates wall material erosion predictions and comparisons of ablation, conduction, and erosion profiles as a function of time, travel (customer-selected 27, 61, 86, 130, and 201 inches from the rear face of the tube (RFT)), and number of rounds to barrel condemnation. The A723 steel and 0.005-inch high contraction (HC) chromium plated/A723 steel wall materials are evaluated for maximum wall temperature and erosion. The MACE code can do any propellant-gun barrel combination on a high-end PC, each mechanism's importance is identified, and incremental upgrades are feasible.

RESULTS AND DISCUSSION

Figure 1 provides a gun erosion modeling overview that includes the bore surface erosion analysis using the ABAQUS, XNOVAKTC, CCET, MABL, and MACE codes. In addition, this figure provides an overview of the subsurface erosion analysis using metallographic data and the XNOVAKTC, CCET, MABL, and MACE codes.

Figure 2 gives the calculated ambient temperature-conditioned M829A2 XNOVAKTC gas pressures (P) as a function of time for the customer-selected axial positions. Figure 3 gives the calculated ambient temperature-conditioned M829A2 XNOVAKTC gas temperatures (T) as a function of time for these same positions. Figure 4 gives the calculated ambient temperature-conditioned M829A2 XNOVAKTC gas velocities (V) as a function of time, again for these same positions. For Figure 4, the y-axis is qualitatively presented, since muzzle velocity-related data require both a clearance and need to know.

Figure 5 gives the calculated ambient temperature-conditioned M829A2 MABL recovery enthalpies (H_r) as a function of time for the same customer-selected axial positions above. Figure 6 gives the calculated ambient temperature-conditioned M829A2 MABL cold wall heat flux (Q_{cw}) as a function of time for these same positions. The data in Figures 5 and 6 are two of three parts of the driving potential ($Q_{cw}/(H_r-H_{gw})$), which is essentially mass affected per unit area per unit time.

Figure 7 gives the calculated M829A2 CCET reacting wall enthalpies (H_w) for HC chromium plated and A723 walls as a function of temperature. The figure includes the third of three parts of the driving potential ($Q_{cw}/(H_r-H_{gw})$), which again is essentially mass affected per unit area per unit time. Figure 8 gives the calculated M829A2 CCET ablation and melting potential (B_a) for HC chromium plated and A723 walls as a function of temperature.

Figures 7 and 8 show that the HC chromium plated wall oxidizes at 3600°R (3110°F), it has a solid-solid transformation at 3790°R (3300°F), it melts at 3830°R (3340°F), and its oxide melts at 4570°R (4080°F). Figures 7 and 8 show that the A723 wall has a solid-solid transformation at 1800°R (1310°F), it oxidizes at 1900°R (1410°F), its oxide melts at 2960°R (2460°F), and it melts at 3250°R (2760°F). These two figures show that the highly reactive

A723 wall oxidizes and expansively flakes substantially below its melting point, while the nearly inert HC chromium plated wall oxidizes and passivates just below its higher melting point. In addition, these two figures show that the highly susceptible A723 wall oxide melts well below its mostly iron metal, while the much less susceptible HC chromium plated wall oxide melts well above chromium metal.

Figure 9 shows the M829A2 27-inch RFT inhibited growth fit of subsurface exposure test data of gun barrels removed from service. The percentage of subsurface A723 area exposed through the HC chromium plate is plotted against EFC M829A2 rounds for a typical low-round example and a typical high-round example. The primary damage mechanism is cyclic thermal-induced evolution of water, oxygen, hydrogen, chlorine, and other impurities from their trapped states leading to exponential growth of HC chromium plate shrinkage and heat-check cracking before leveling off at 10 percent of the gun's erosion life. Shrinkage and cracking lessen with increased travel. The HC chromium plate has no phase change shrinkage. It starts (as manufactured) with a fine crack network (finite shrinkage) at round zero and levels off to a "maximum" shrinkage at approximately 10 percent of the gun's erosion life for EFC M829A2 rounds.

Heat-checked HC chromium plate pits and chips from mechanical bourrelet abrasion and high velocity gas flow. For the M256 gun barrel using long rod penetrator rounds, Higgins (ref 15) first showed a large front bourrelet (both aluminum and composite types) radial contact force at 65 to 85 inches from the RFT. Simkins (ref 16) first showed maximum traveling wave resonance contact force at and near the muzzle.

The morphology of this crack network in electrodeposited chromium can be altered by current density, deposition temperature, catalyst type, bath concentrations, and other parameters. The chromium plate used for U.S. Army-manufactured guns is a chromium alloy with a low atomic percentage of oxygen, hydrogen, and chlorine, as well as other trace elements.

Initial production of 120-mm M256 gun tubes gave widely variable HC chromium plate quality due to inadequate HC chromium plating process control. It took a few years to develop an adequate HC chromium plating process control drawing that detailed enhancements in tube preparation, anode preparation, multiple bath preparation, rinsing between baths, and time between baths.

Current production of 120-mm M256 gun tubes gives mildly variable HC chromium plate quality within the many parameter tolerances of the HC chromium plating process control drawing. The experimentally-observed mild variation in the maximum shrinkage of HC chromium plate for a given number of EFC M829A2 rounds may be attributed to this in-tolerance variation.

Actual inspections of HC and low contraction (LC) chromium plated A723 samples indicate that 120-mm M256 gun tubes may have significantly less variable LC chromium plate quality than the above HC chromium plate quality within the many parameter tolerances of the HC chromium plating process control drawing. One positive attribute of LC chromium plate is that it is typically 0.003-inch thicker than HC chromium plate, 0.008-inch versus 0.005-inch. The MACE code predicts an LC chromium plate/A723 steel interface temperature of approximately 400°F below the HC chromium plate/A723 steel interface temperature.

Based on limited data, another positive attribute of LC chromium plate is that the experimentally-observed initial shrinkage due to manufacturing and maximum shrinkage due to firings (both a function of crack network) are significantly less than that of HC chromium plate. Due to limited the data, it is too early to definitively state the degree that LC chromium plated gun steel will out-perform HC chromium plated gun steel.

Figure 10 shows two typical HC chromium plated A723 steel depth profile examples of M829A2 relative rounds-to-plate spalling based on subsurface exposure and flow modeling at 27 inches from RFT. The secondary damage mechanism is A723 thermochemical gas wash at heat-checked crack bases and after HC chromium platelet spalling, which enhances pitting and chipping by mechanical forces. Scattered HC chromium platelet spalling gives the common pitted appearance seen near erosion onset. The overall HC chromium plate is 0.005-inch thick, and chromium platelets are the individual pieces of the chromium plate resulting from heat-checking.

The upper portion of Figure 10 gives a typical low-round example depth profile with 12.9 percent subsurface exposed and 1.0x relative average rounds calculated to chromium plate spalling with respect to the typical high-round example depth profile. The lower portion of this figure gives a typical high-round example depth profile with 6.35 percent subsurface exposed and 2.1x relative average rounds calculated to chromium plate spalling with respect to the typical low-round example depth profile.

Figure 10 depicts 1.0x and 2.1x respective rounds for a pair of appropriate-sized subsurface A723 voids to occur at adjacent cracks, thus causing the HC chromium platelet to spall due to the consumption of a critical area under the HC chromium platelet. The exposed area of subsurface A723 varies with interface driving potential, heat transfer, and temperature. These average geometries are valid for the last 90 percent of gun erosion life for EFC M829A2 rounds. Data for these typical low- and high-round examples were acquired from metallographical analysis of gun barrels removed from service. Actual gun barrel data are necessary, since no known thermomechanical crack model exists for guns.

Figure 11 gives the calculated MACE ambient temperature-conditioned M829A2 maximum wall and interface temperatures as a function of the axial position from the RFT. This figure shows the MACE code-generated 0.005-inch HC chromium wall with slightly passivated surface oxide, on A723 steel. The top curve is very slightly oxidized/passivated at 27 inches,

unreacted at the other four positions (61, 86, 130, and 201 inches), and unmelted at all five positions. The slight surface oxide mildly reduces heat transfer to the HC chromium wall.

Figure 11 also shows the MACE code-generated A723 steel wall (after chromium plate spalling). The second curve is oxidized (expansive flaking type) at 27 inches, not applicable at the other four positions (61, 86, 130, and 201 inches) in the gun's life with this round type unless mechanical pitting and chipping occur, and unmelted at all five positions. At 27 inches from RFT, heat-checked crack bases are A723 thermochemically gas washed, spalling HC chromium platelets. At the other four positions, HC chromium is not spalled by A723 thermochemical crack base gas washing, but may pit and chip by mechanical forces. At 61 and 86 inches from RFT, A723 thermochemical gas wash is rapid after HC chromium platelet mechanical loss since the iron oxide is melting in a high velocity flow environment.

Figure 11 further shows the MACE code-generated A723 steel wall typical low-round example at the chromium plate interface. The third curve is oxidized (expansive flaking type) at 27 and 61 inches, unreacted at 86, 130, and 201 inches, and unmelted at all five positions. This figure also shows the MACE code-generated A723 steel wall typical high-round example at the chromium plate interface. The last curve is oxidized (expansive flaking type) at 27 and 61 inches, unreacted at 86, 130, and 201 inches, and unmelted at all five positions.

It is clearly shown in Figure 11 that all A723 steel-comprised data exceeded both the 1310°F A723 steel solid-solid transformation and the 1410°F A723 steel iron oxidation temperatures at the 27 and 61-inch positions, but not at the 86, 130, and 201-inch positions. The figure also shows that all A723 steel-comprised data do not exceed either the 2460°F A723 steel iron oxide solid-liquid transformation or the 2760°F A723 steel iron solid-liquid transformation temperatures at any position.

Figure 12 gives the calculated MACE ambient temperature-conditioned M829A2 cumulative wall erosion depth-to-condemnation as a function of EFC ambient temperature-conditioned M829A2 rounds. The curves will be discussed in order of increasing rounds to condemnation. The first curve at 27 inches from RFT is a typical low-round example, where the A723 gas wash onset is at 224 rounds (interface degrades, HC chromium begins spalling platelets forming pits) and erosion condemnation is at 275 rounds. The second curve at 27 inches from RFT is a typical high-round example, where the A723 gas wash onset is at 455 rounds (interface degrades, HC chromium begins spalling platelets forming pits) and erosion condemnation is at 506 rounds. The third curve in Figure 12 at 61 inches from RFT is a typical low-round example, where at 500 rounds it is 18 percent to A723 gas wash onset. The last curve at 61 inches from RFT is a typical high-round example, where at 500 rounds it is 4 percent to A723 gas wash onset.

MACE predictions are through 1500 rounds. Unless mechanical pitting or chipping occurs, the 0.005-inch HC chromium wall is uneroded at 27, 61, 86, 130, and 201 inches from RFT. Also the A723 interface is uneroded at 86, 130, and 201 inches from RFT unless

mechanical pitting or chipping occurs. At both 61 and 86 inches from RFT, if HC chromium mechanically pits or chips, then thermochemical A723 gas wash is five times more severe than at 27 inches from RFT. At 201 inches from RFT, if HC chromium mechanically pits or chips, then thermochemical A723 gas wash is virtually nonexistent.

Figure 12 indicates from the U.S. Army technical manual on evaluation of cannon tubes (ref 17) that the 120-mm M256 gun erosion condemnation criterion is when A723 gas wash first exceeds 5-mm or 0.200-inch in depth at any location measured by the standard radial arm erosion gauge. The figure also indicates the 120-mm M256 gun fatigue condemnation criterion or safe service life of 1500 EFC rounds, where all rounds have an EFC factor of one.

Officially from the Army technical manual (ref 17), erosion results when the chromium plating on the bore is lost (light chrome pitting and chipping of the bore) and hot propellant gases wash across the unprotected base metal of the tube bore (heavy chrome chipping of the bore with some light bore erosion). Erosion is detected and its location is determined by use of a borescope. The depth of erosion is measured using a bore erosion gauge. Although the 120-mm M256 gun is condemned on the first occurrence of either the erosion or the fatigue criterion, it is very rare that the latter dominates.

Figure 13 shows that 120-mm M256/M829A2 erosion modeling predictions concur with the typical wear and erosion pattern of retired M256 gun barrels with significant numbers of M829A2 rounds. This typical wear and erosion pattern of retired M256 gun barrels with significant numbers of recorded M829A2 rounds includes three locations of wear and erosion. Retired M256 tubes typically have firing mixtures of M829A2, M829A1, M829, and/or other round types that are cold, ambient, and hot temperature-conditioned before firing for each round type. The retired M256 tubes typically have a total of approximately 200 to 800 rounds with approximately 100 to 400 M829A2 rounds.

For retired M256 gun barrels with significant numbers of recorded M829A2 rounds, the first location of wear and erosion occurs approximately 24 to 60 inches from RFT and includes uniform severe heat-checking and uniform scattered pitting with mild A723 loss that diminishes for this region with increased travel. The forcing cone ends at approximately 24 inches from the RFT.

Also for retired M256 gun barrels with significant numbers of recorded M829A2 rounds, the second location of wear and erosion occurs approximately 65 to 85 inches from the RFT and includes mild heat-checking, uniform scattered pitting, and a few to a few dozen uniform scattered deep scoring holes that are all independent of travel for this region. Any scoring hole 5-mm deep will condemn the M256 tube, and the 5-mm depth obviously involves substantial A723 loss.

Finally, for retired M256 gun barrels with significant numbers of recorded M829A2 rounds, the third location of wear and erosion occurs in the last 2 to 3 feet of travel at the muzzle and includes very mild heat-checking and uniform scattered HC chromium plate loss with virtually no A723 loss that are all independent of travel for this region.

REFERENCES

1. von Karman, T., *Sorbonne Lectures*, 1951-1952; see also *Princeton University Lectures*, 1953; "Fundamental Approach to Laminar Flame Propagation," *AGARD Selected Combustion Problems*, Butterworths, London, 1954; and "Fundamental Equations in Aerothermochemistry," *Proc. 2nd AGARD Combust. Colloq.*, Liege, Belgium, 1955.

2. Reshotko, E., and Cohen, C.B., "Heat Transfer at the Stagnation Point of Blunt Bodies," NACA TN Number 3513, 1955.

3. Cohen, C.B., Bromberg, R., and Lipkis, R.P., "Boundary Layers with Chemical Reactions Due to Mass Additions," Report No. GM-TR-268, The Ramo-Wooldridge Corporation, Los Angeles, CA, 1957.

4. Denison, M.R., and Dooley, D.A., "Combustion in the Laminar Boundary Layer of Chemically Active Sublimators," Publication No. C-110, Aeronutronic Systems, Inc., Glendale, CA, 1957.

5. Lees, L., "Convective Heat Transfer with Mass Addition and Chemical Reactions," *Combustion and Propulsion, Proc. 3rd AGARD Combust. Colloq.*, Palermo, Sicily, Pergamon Press, NY, 1958; see also *Recent Advances in Heat and Mass Transfer*, McGraw-Hill, NY, 1961.

6. Nickerson, G., Berker, D., Coats, D., and Dunn, S., "Two-Dimensional Kinetics (TDK) Nozzle Performance Computer Program," Software and Engineering Associates, Inc., Carson City, NV, 1993.

7. Dunn, S., "Materials Ablation Conduction Erosion Program (MACE)," Software and Engineering Associates, Inc., Carson City, NV, 1989.

8. Gordon, S., and McBride, B., "Computer Program for Calculation of Complex Chemical Equilibrium Compositions, Rocket Performance, Incident and Reflected Shocks, and Chapman-Jouguet Detonations (CET)," NASA SP-273, NASA Lewis Research Center, Cleveland, OH, 1971.

9. Picard, J., Ahmad, I., and Bracuti, A., *Proceedings of the Tri-Service Gun Tube Wear and Erosion Symposiums*, U.S. Army ARDEC/ADPA, Dover, NJ, 1970, 1972, 1977, and 1982.

10. Alkidas, A., Morris, S., Christoe, C., Caveny, L., and Summerfield, M., "Erosive Effects of Various Pure and Combustion-Generated Gases on Metals - Part II," Technical Report, U.S. Army Materials and Mechanics Research Center, Watertown, MA, 1977; see also Part I, 1975.

11. Freedman, E., "BLAKE - A Thermodynamic Code Based on Tiger: User's Guide and Manual," Technical Report ARBRL-TR-02411, U.S. Army Ballistic Research Laboratory, Aberdeen Proving Ground, MD, 1982.

12. Gough, P., "The XNOVAKTC Code," Paul Gough Associates, Portsmouth, NH, 1990.

13. Dunn, S., Sopok, S., Coats, D., O'Hara, P., Nickerson, G., and Pflegl, G., "Unified Computer Model for Predicting Thermochemical Erosion in Gun Barrels," *Proceedings of 31st AIAA Joint Propulsion Conference*, San Diego, CA, July, 1995.

14. *ABAQUS Manual*, Hibbitt, Karlsson & Sorensen, Inc., Pawtucket, RI, 1996.

15. Higgins, J. "Investigation of the Effect of Projectile/Tube Interaction on Cannon Bore Erosion in the M256 Tank Gun System," Memorandum Report, U.S. Army Benet Laboratories, Watervliet, NY, 1995.

16. Simkins, T., "Traveling Wave Resonance in Gun Tubes," U.S. Army ARDEC Technical Report ARCCB-TR-87028, Benet Laboratories, Watervliet, NY, October 1987.

17. *Evaluation of Cannon Tubes*, U.S. Army Technical Manual No. TM 9-1000-202-14, Headquarters, Department of the Army and Air Force, Washington, DC, June 1993.

Figure 1 - Gun Erosion Modeling Overview

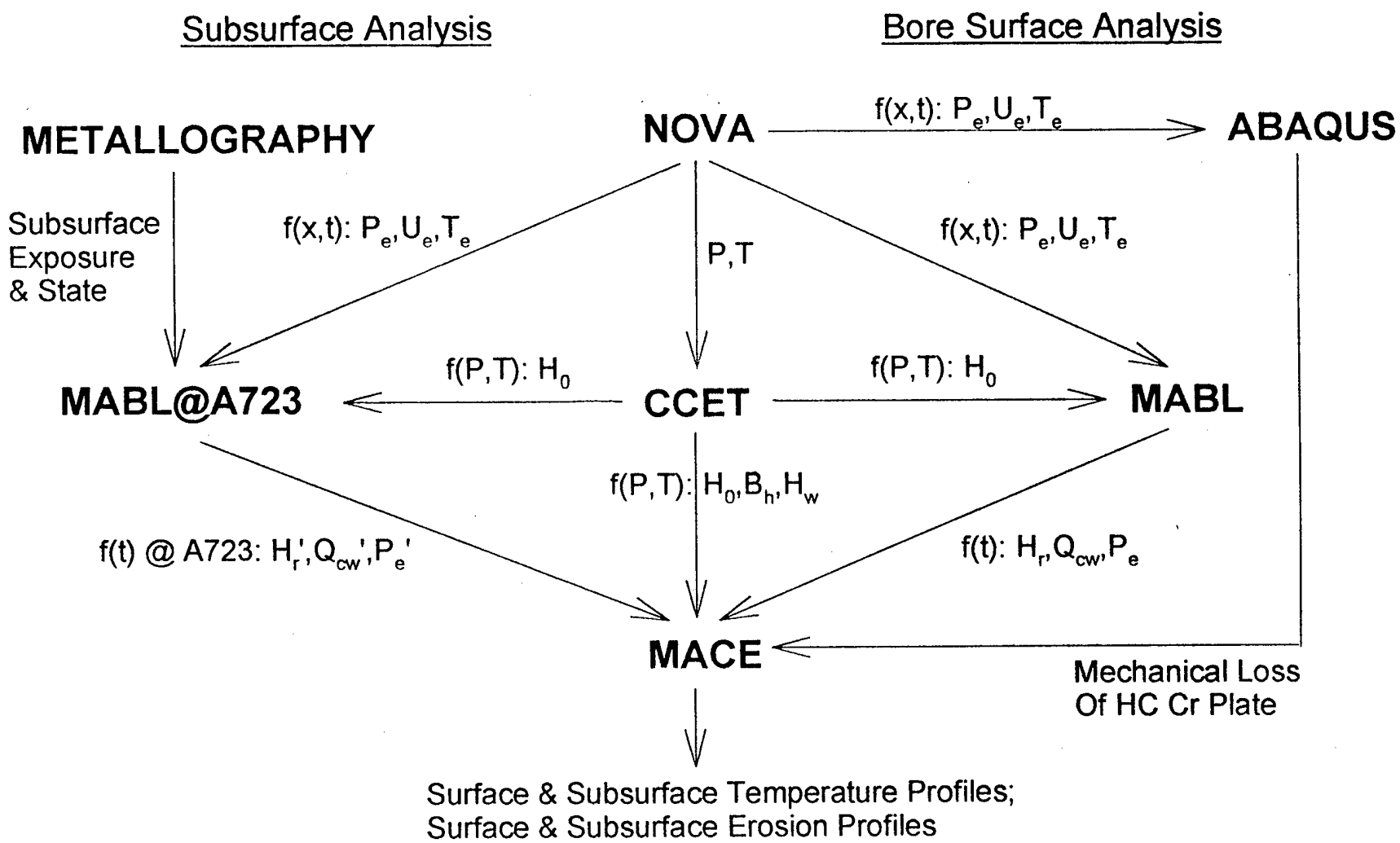

Figure 2 - Ambient Conditioned M829A2 XNOVAKTC Gas Pressures

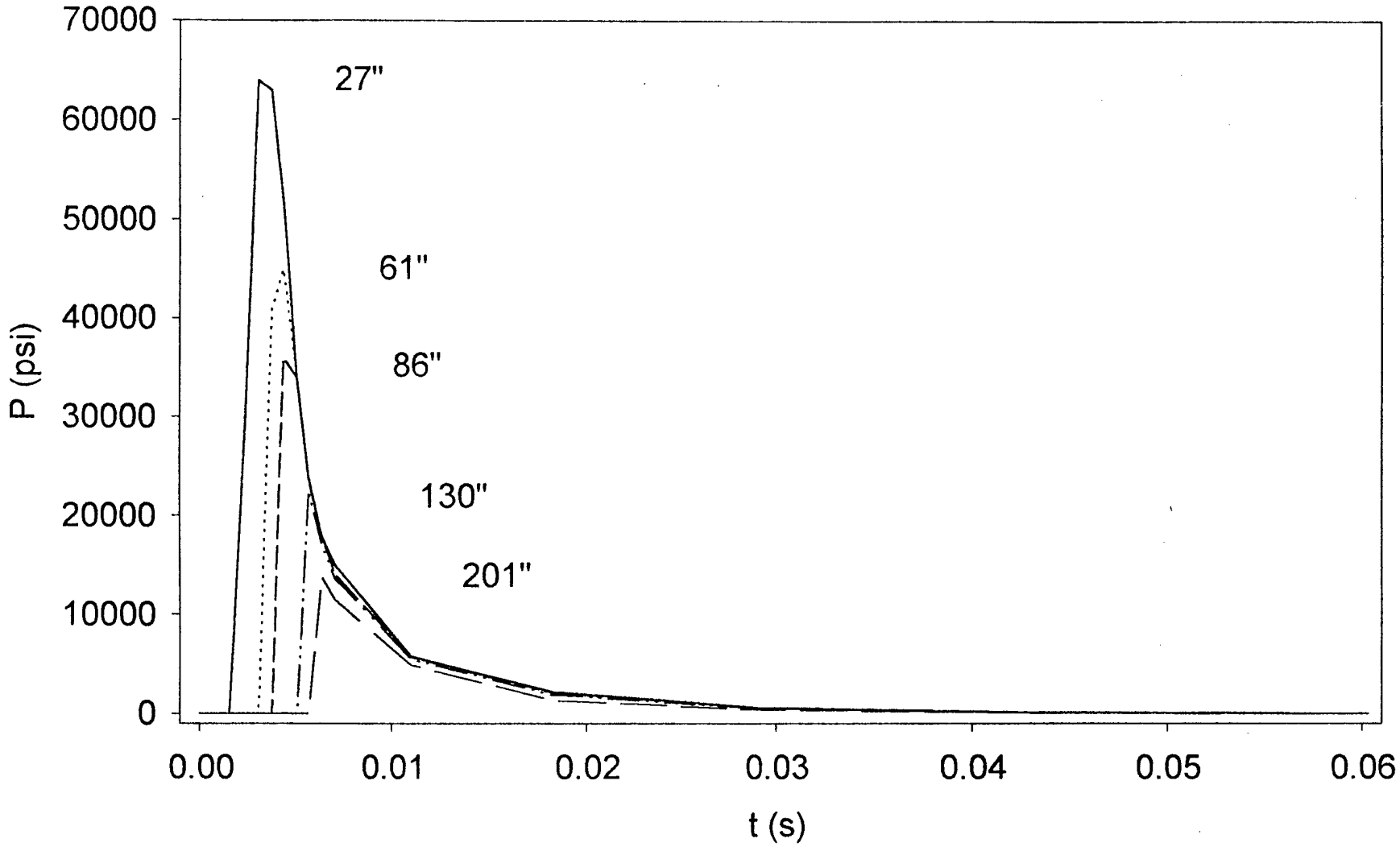

Figure 3 - Ambient Conditioned M829A2 XNOVAKTC Gas Temperatures

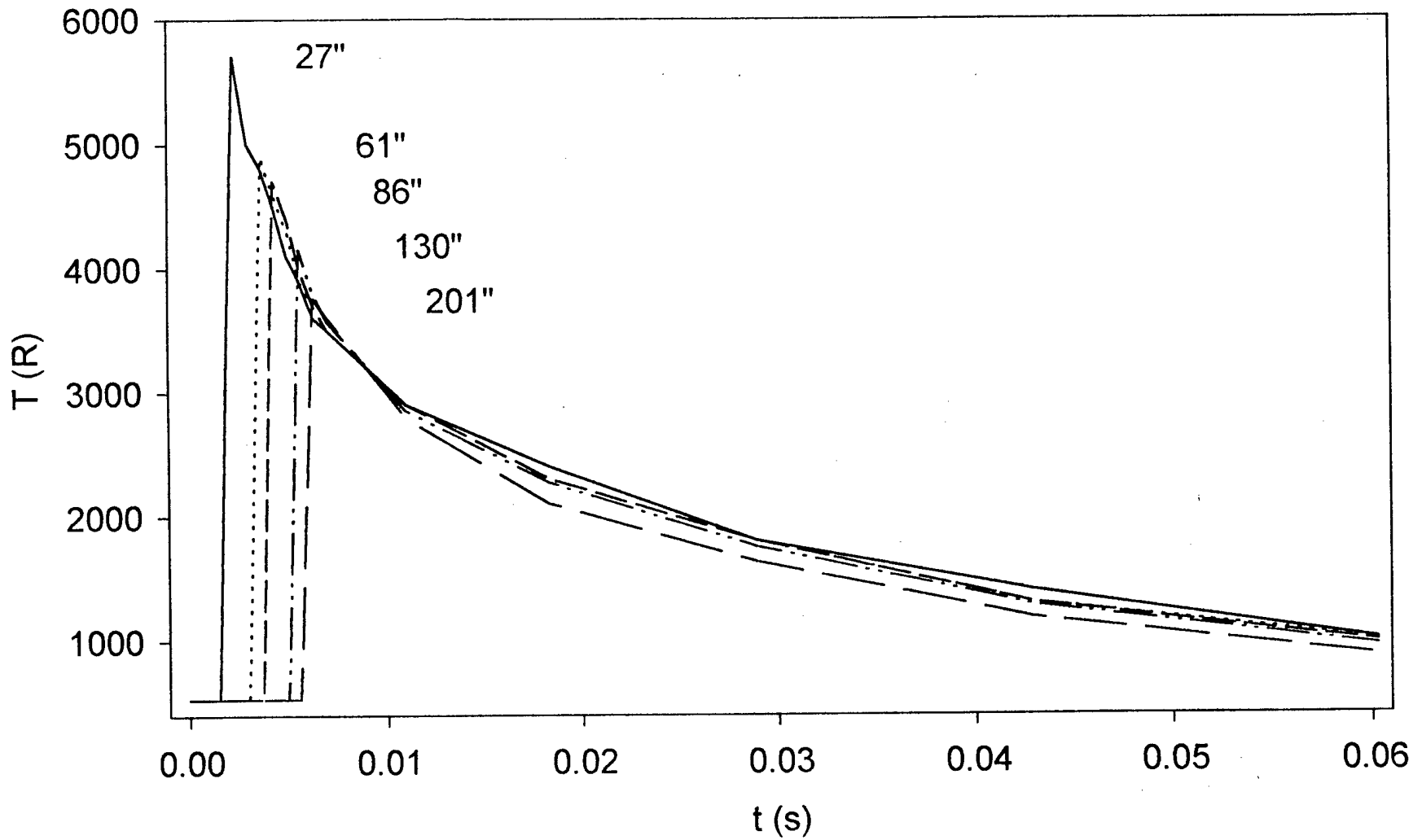

Figure 4 - Ambient Conditioned M829A2 XNOVAKTC Gas Velocities

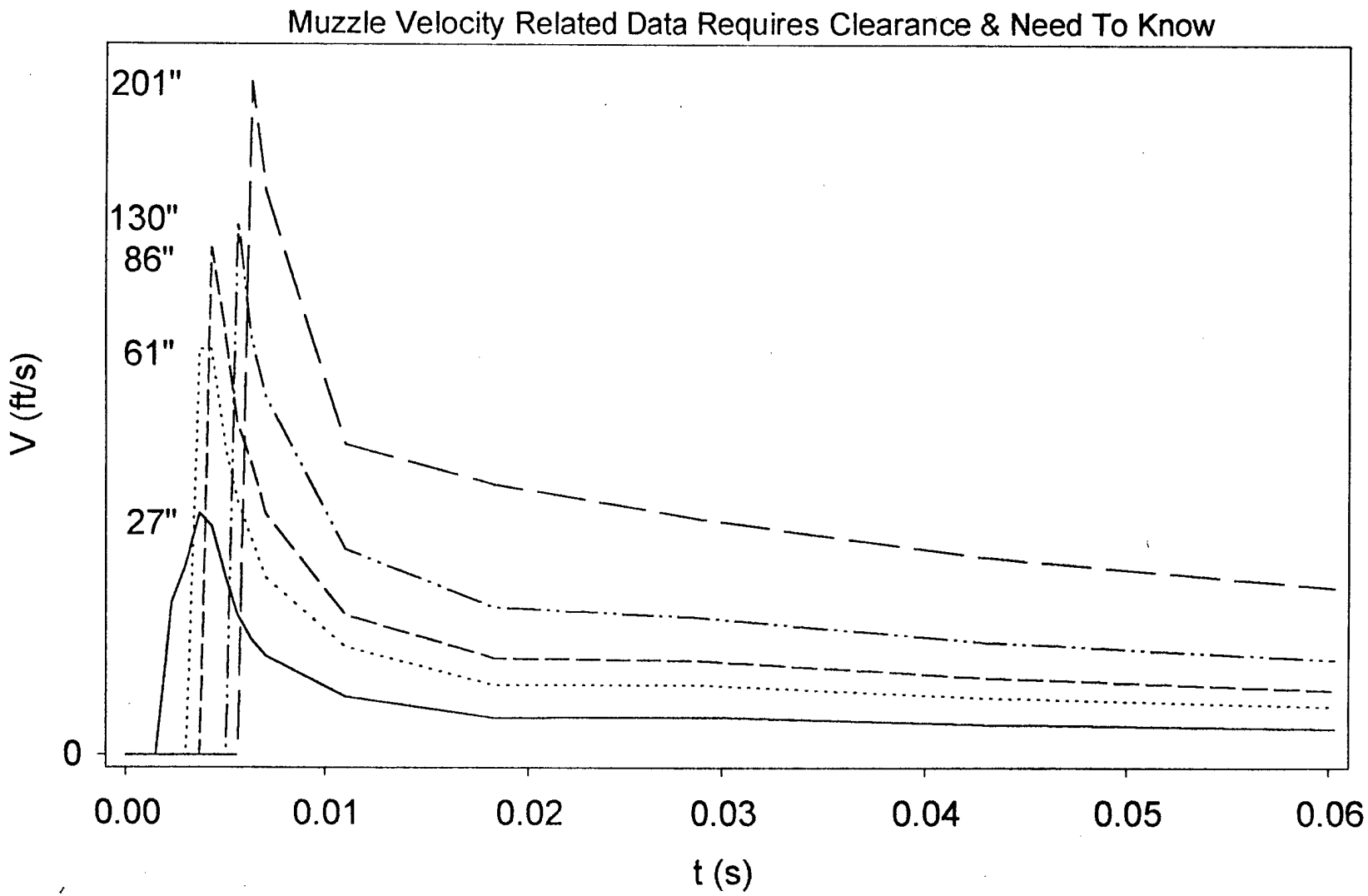

Figure 5 - Ambient Conditioned M829A2 MABL Recovery Enthalpies

$Q_{ow} / (H_r - H_{gw})$ = Mass Removal / Area Time = Driving Potential

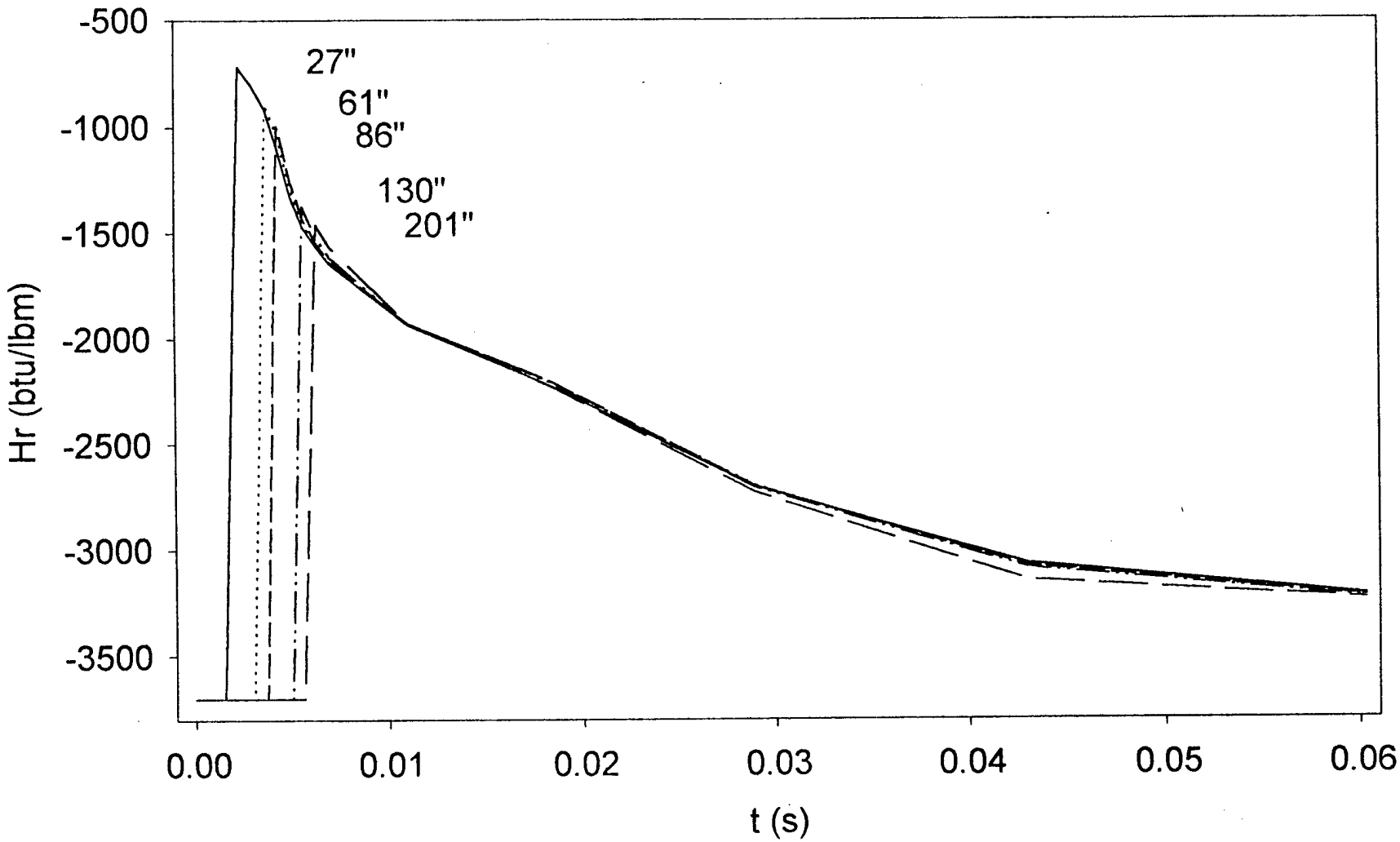

Figure 6 - Ambient Conditioned M829A2 MABL Cold Wall Heat Flux

Q_{cw} / (H_r-H_{gw}) = Mass Removal / Area Time = Driving Potential

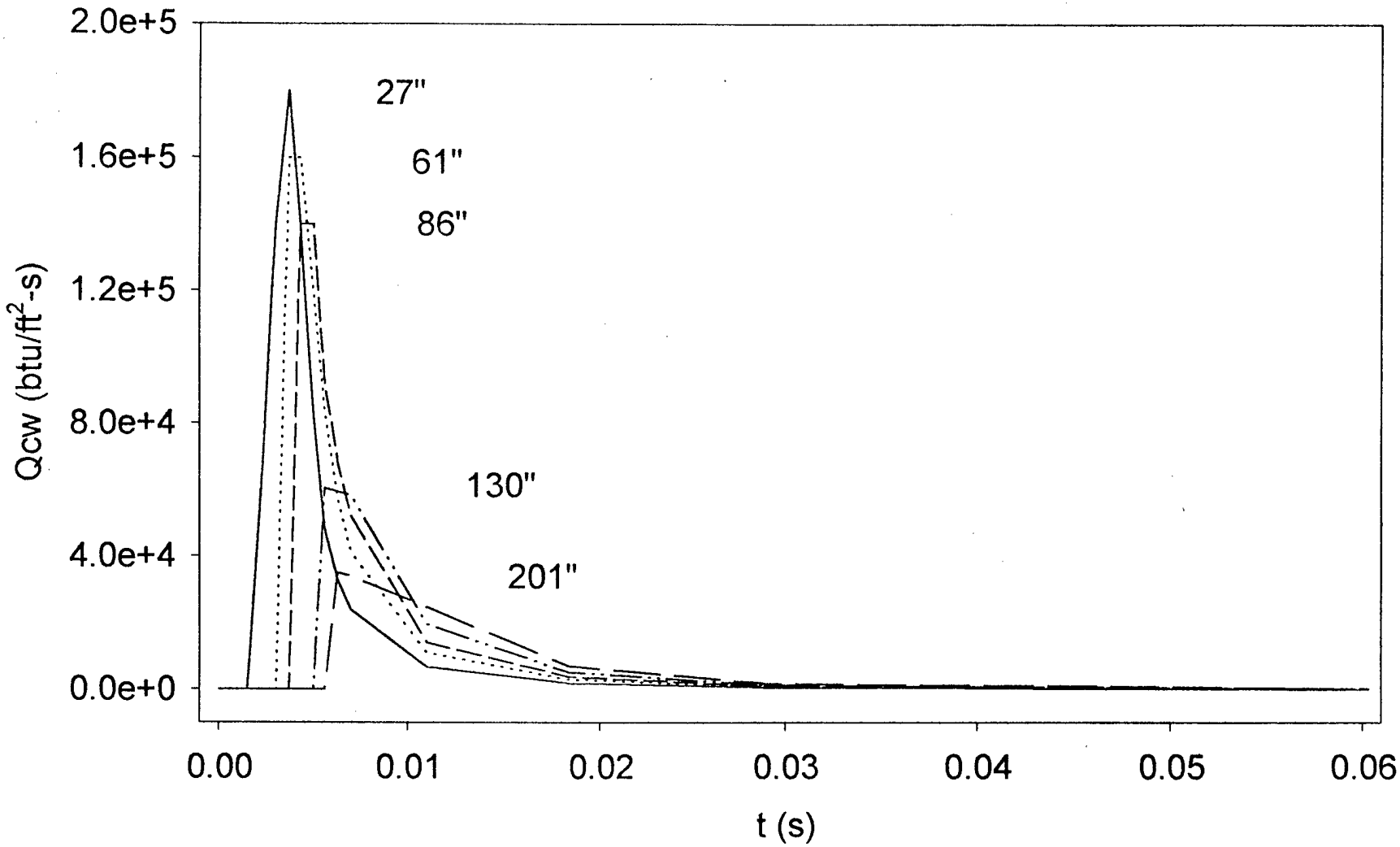

Figure 7 - M829A2 CCET Reacting Wall Enthalpies

$Q_{cw} / (H_r - H_{gw})$ = Mass Removed / Area Time = Driving Potential

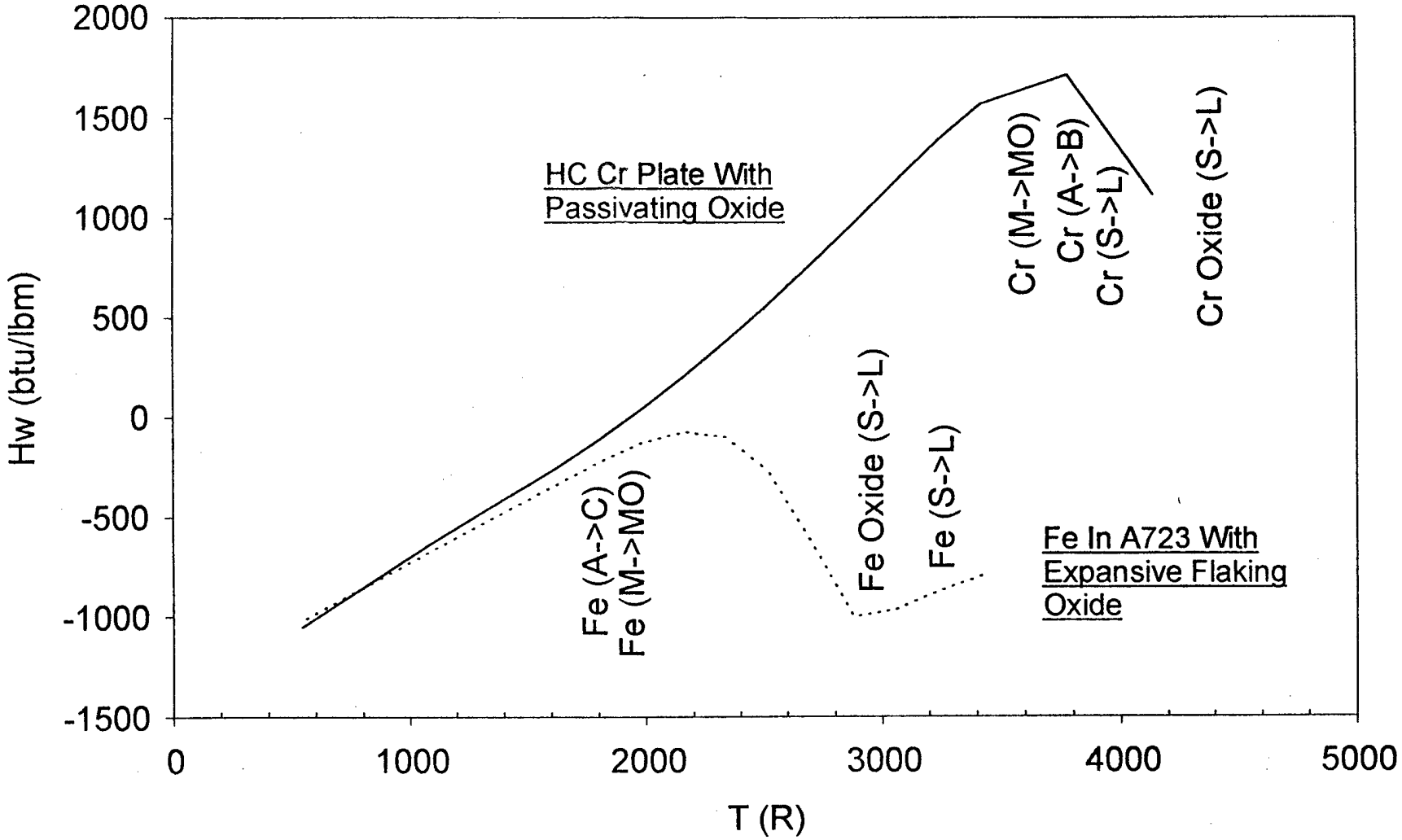

Figure 8 - M829A2 CCET Ablation & Melting Potential

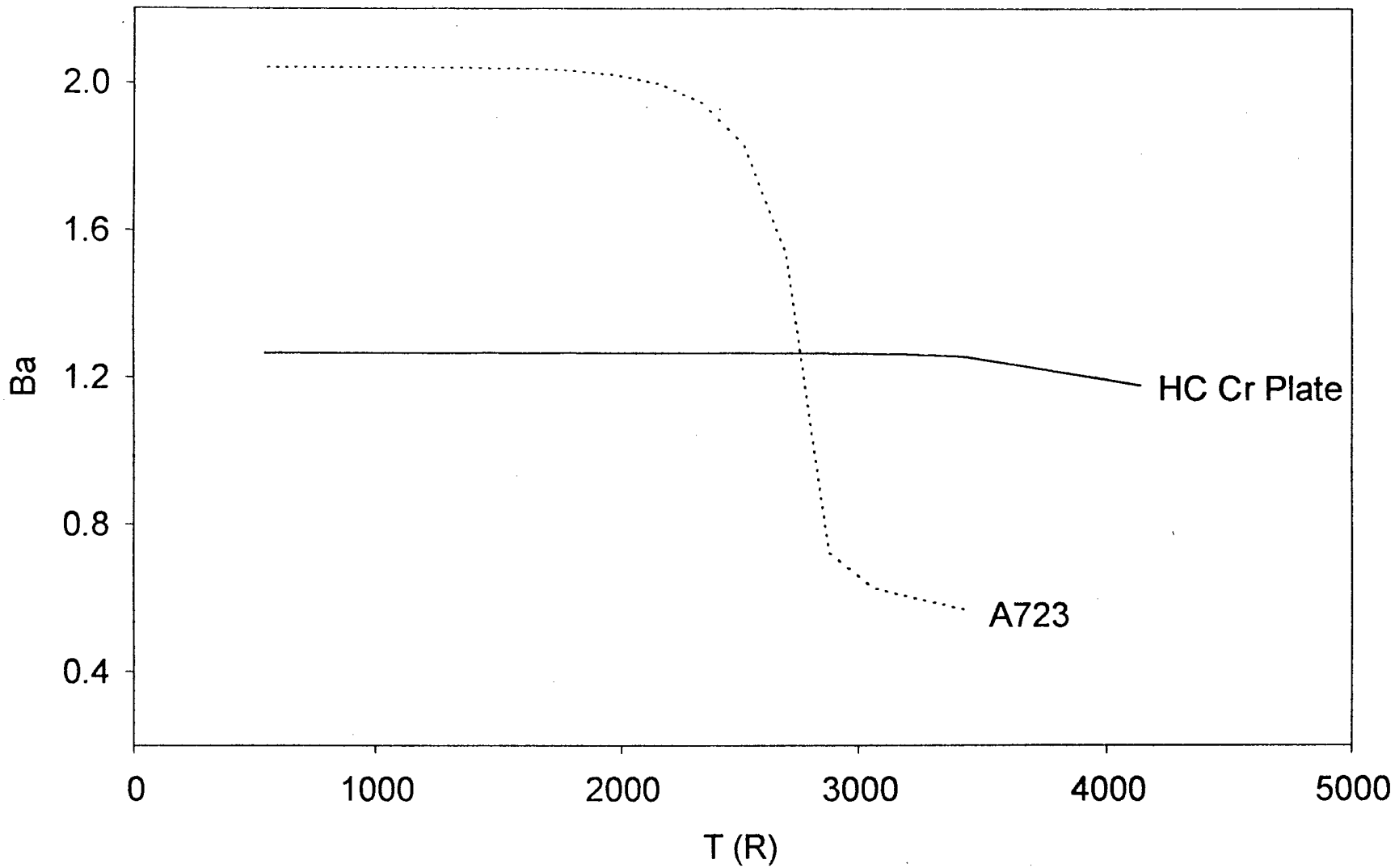

Figure 9 - M829A2 27" RFT Inhibited Growth Fit Of Subsurface Exposure Test Data

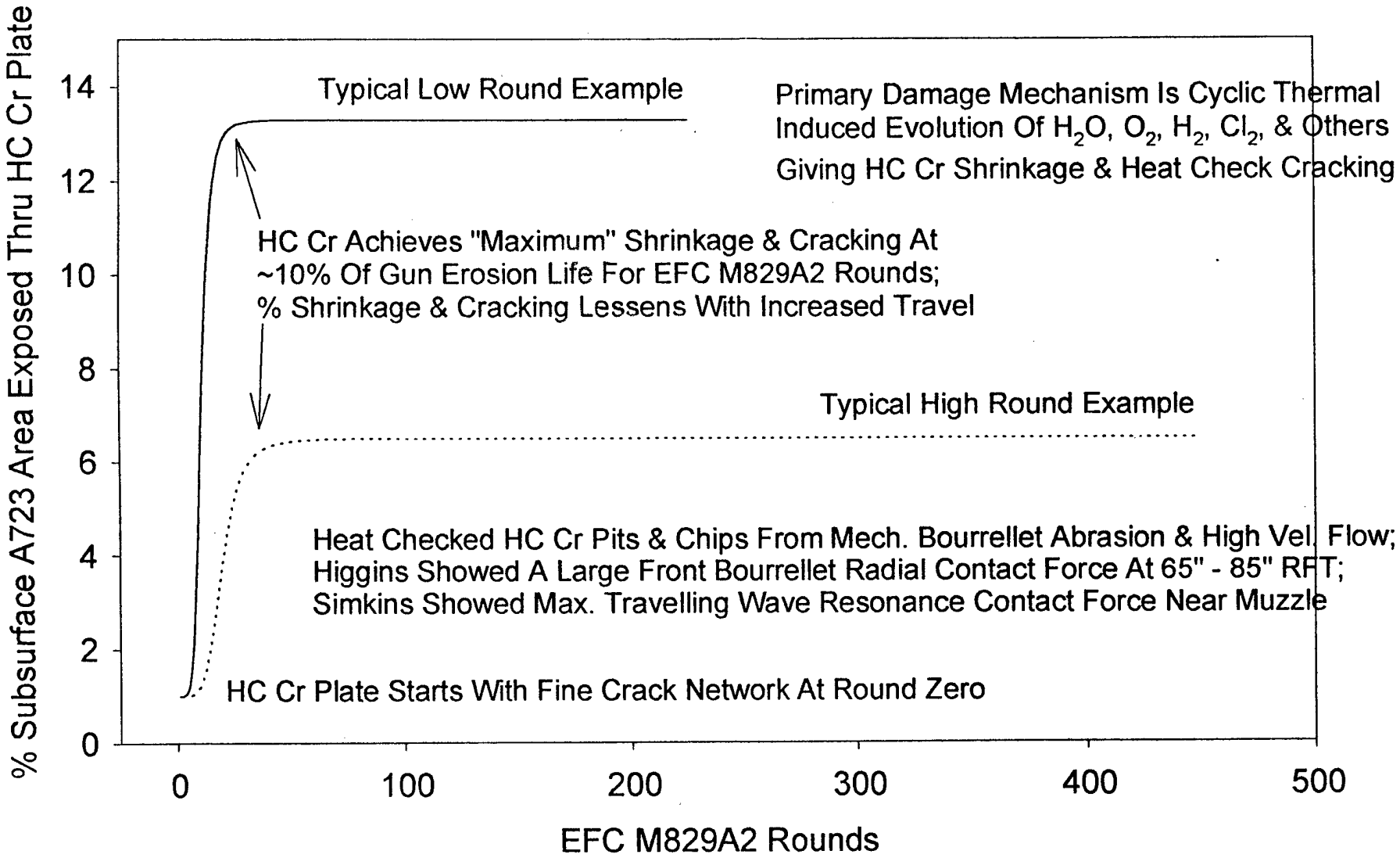

Figure 10 - M829A2 Typical Relative Rounds To Plate Spalling Based On Subsurface Exposure & Flow Modeling At 27" RFT

Secondary Damage Mechanism Is A723 Thermochemical Gas Wash At Heat Checked Crack Bases And After HC Cr Platelet Spalling Which Enhances Pitting & Chipping By Mech. Forces

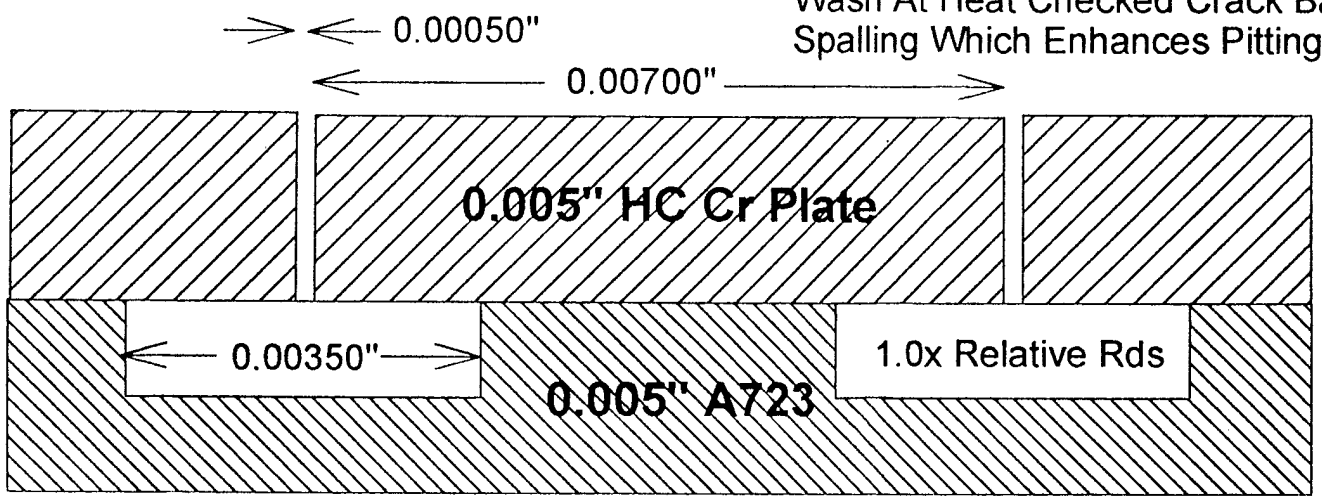

Typical Low Round Example;
12.9% Subsurface Exposed;
1.0x Rel Ave Rds To Spalling

These Average Geometries Are Valid For Last 90% Of Gun Life For EFC M829A2 Rounds

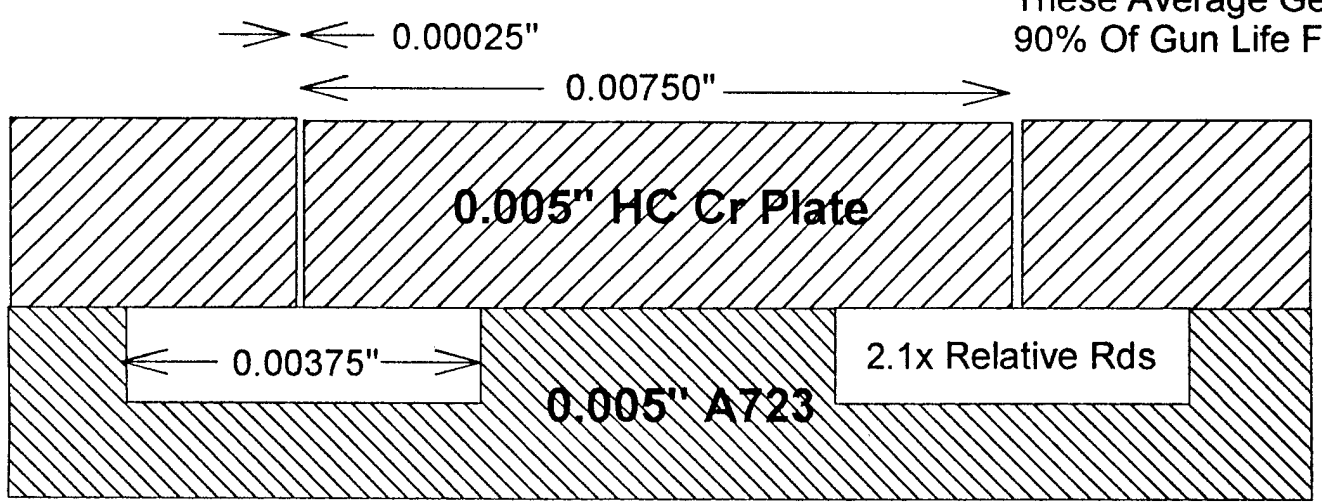

Typical High Round Example;
6.35% Subsurface Exposed;
2.1x Rel Ave Rds To Spalling

Figure 11 - MACE Ambient Cond. M829A2 Maximum Wall & Interface Temperatures

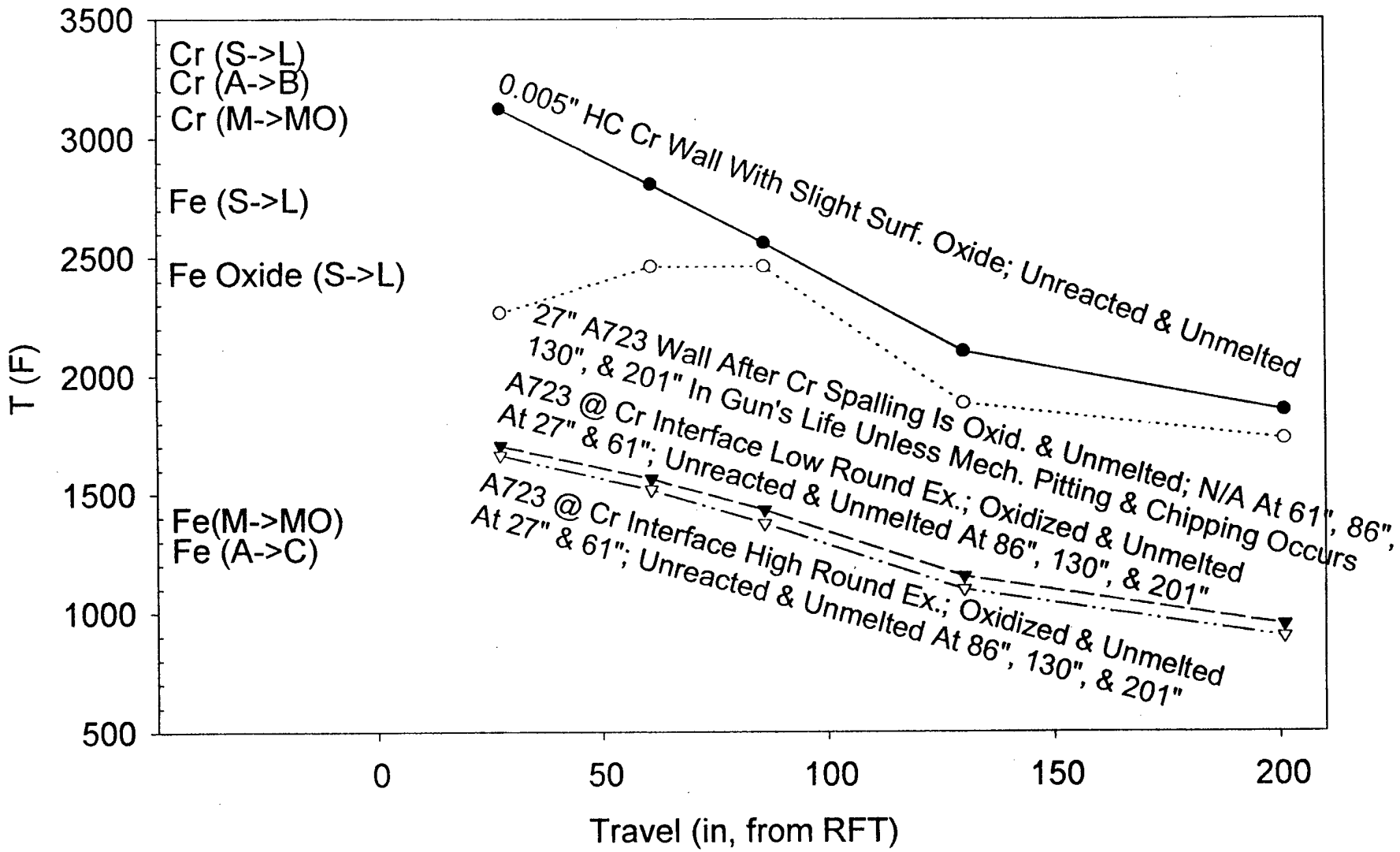

Figure 12 - MACE Ambient Cond. M829A2 Cumulative Wall Erosion To Condemnation

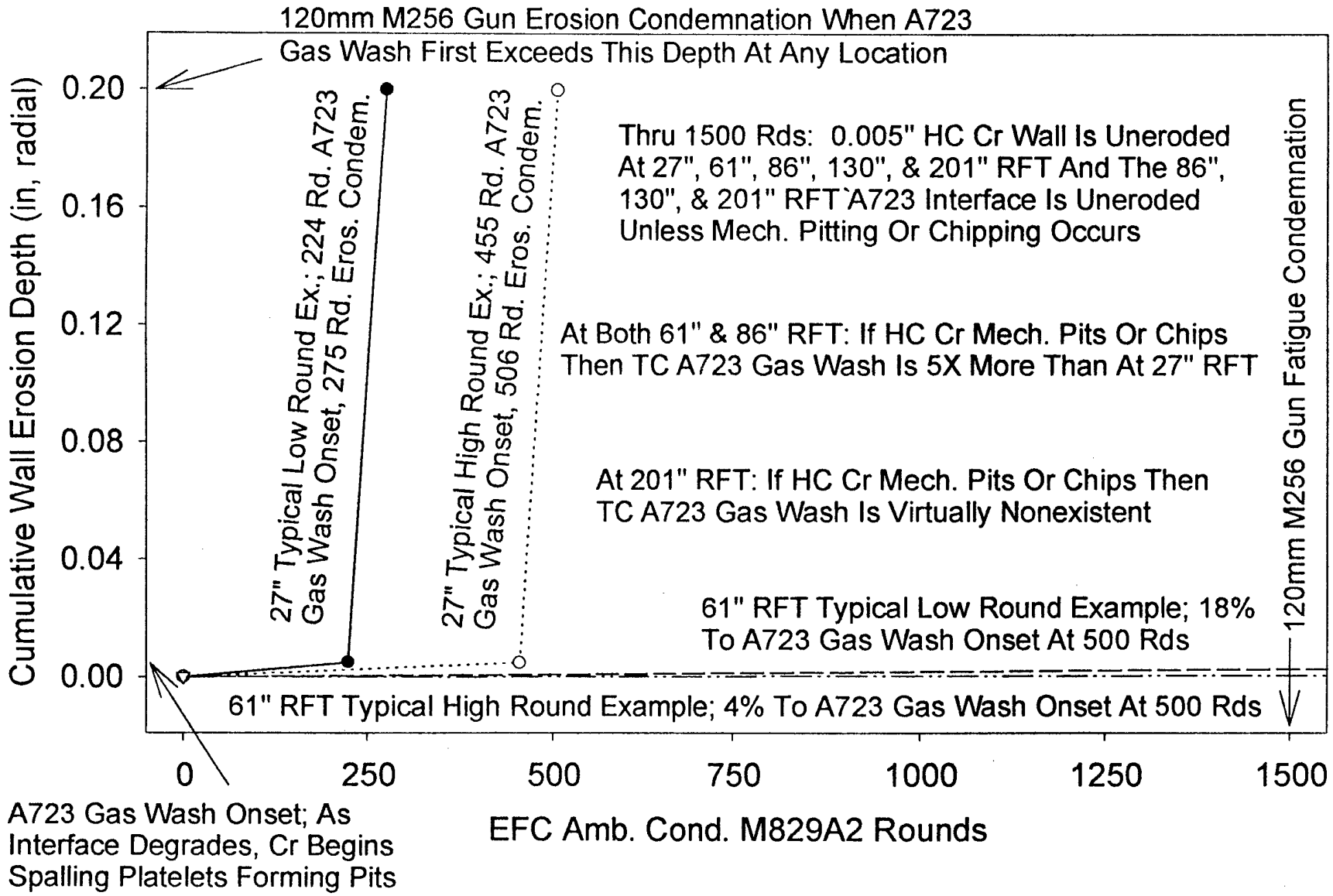

Figure 13 - 120mm M256/M829A2 Erosion Modeling Concurs With The Typical Wear & Erosion Pattern Of Retired M256 Gun Barrels With M829A2 Rounds

At ~24"-60" RFT:

Uniform Severe Heat Checking; Decr. With Travel
Uniform Scattered Pitting With Mild A723 Loss; Decr. With Travel

At ~65"-85" RFT:

Mild Heat Checking & Uniform Scattered Pitting; Both Indep. Of Travel
1 - 30 Uniform Scattered Deep Scoring Holes; Indep. Of Travel; (Higgins)

At & Near Muzzle:

Very Mild Heat Checking; Indep. Of Travel
Uniform Scattered HC Cr Loss w/o A723 Loss; Indep. Of Travel; (Simkins)

TECHNICAL REPORT INTERNAL DISTRIBUTION LIST

	NO. OF COPIES
CHIEF, DEVELOPMENT ENGINEERING DIVISION	
ATTN: AMSTA-AR-CCB-DA	1
-DB	1
-DC	1
-DD	1
-DE	1
CHIEF, ENGINEERING DIVISION	
ATTN: AMSTA-AR-CCB-E	1
-EA	1
-EB	1
-EC	1
CHIEF, TECHNOLOGY DIVISION	
ATTN: AMSTA-AR-CCB-T	2
-TA	1
-TB	1
-TC	1
TECHNICAL LIBRARY	
ATTN: AMSTA-AR-CCB-O	5
TECHNICAL PUBLICATIONS & EDITING SECTION	
ATTN: AMSTA-AR-CCB-O	3
OPERATIONS DIRECTORATE	
ATTN: SIOWV-ODP-P	1
DIRECTOR, PROCUREMENT & CONTRACTING DIRECTORATE	
ATTN: SIOWV-PP	1
DIRECTOR, PRODUCT ASSURANCE & TEST DIRECTORATE	
ATTN: SIOWV-QA	1

NOTE: PLEASE NOTIFY DIRECTOR, BENÉT LABORATORIES, ATTN: AMSTA-AR-CCB-O OF ADDRESS CHANGES.

TECHNICAL REPORT EXTERNAL DISTRIBUTION LIST

	NO. OF COPIES
ASST SEC OF THE ARMY RESEARCH AND DEVELOPMENT ATTN: DEPT FOR SCI AND TECH THE PENTAGON WASHINGTON, D.C. 20310-0103	1
DEFENSE TECHNICAL INFO CENTER ATTN: DTIC-OCP (ACQUISITIONS) 8725 JOHN J. KINGMAN ROAD STE 0944 FT. BELVOIR, VA 22060-6218	2
COMMANDER U.S. ARMY ARDEC ATTN: AMSTA-AR-AEE, BLDG. 3022	1
AMSTA-AR-AES, BLDG. 321	1
AMSTA-AR-AET-O, BLDG. 183	1
AMSTA-AR-FSA, BLDG. 354	1
AMSTA-AR-FSM-E	1
AMSTA-AR-FSS-D, BLDG. 94	1
AMSTA-AR-IMC, BLDG. 59 PICATINNY ARSENAL, NJ 07806-5000	2
DIRECTOR U.S. ARMY RESEARCH LABORATORY ATTN: AMSRL-DD-T, BLDG. 305 ABERDEEN PROVING GROUND, MD 21005-5066	1
DIRECTOR U.S. ARMY RESEARCH LABORATORY ATTN: AMSRL-WT-PD (DR. B. BURNS) ABERDEEN PROVING GROUND, MD 21005-5066	1
COMMANDER ROCK ISLAND ARSENAL ATTN: SMCRI-SEM ROCK ISLAND, IL 61299-5001	1
COMMANDER U.S. ARMY TANK-AUTMV R&D COMMAND ATTN: AMSTA-DDL (TECH LIBRARY) WARREN, MI 48397-5000	1
COMMANDER U.S. MILITARY ACADEMY ATTN: DEPARTMENT OF MECHANICS WEST POINT, NY 10966-1792	1
U.S. ARMY MISSILE COMMAND REDSTONE SCIENTIFIC INFO CENTER ATTN: AMSMI-RD-CS-R/DOCUMENTS BLDG. 4484 REDSTONE ARSENAL, AL 35898-5241	2
COMMANDER U.S. ARMY FOREIGN SCI & TECH CENTER ATTN: DRXST-SD 220 7TH STREET, N.E. CHARLOTTESVILLE, VA 22901	1
COMMANDER U.S. ARMY LABCOM, ISA ATTN: SLCIS-IM-TL 2800 POWER MILL ROAD ADELPHI, MD 20783-1145	1

NOTE: PLEASE NOTIFY COMMANDER, ARMAMENT RESEARCH, DEVELOPMENT, AND ENGINEERING CENTER, BENÉT LABORATORIES, CCAC, U.S. ARMY TANK-AUTOMOTIVE AND ARMAMENTS COMMAND, AMSTA-AR-CCB-O, WATERVLIET, NY 12189-4050 OF ADDRESS CHANGES.

TECHNICAL REPORT EXTERNAL DISTRIBUTION LIST (CONT'D)

	NO. OF COPIES
COMMANDER U.S. ARMY RESEARCH OFFICE ATTN: CHIEF, IPO P.O. BOX 12211 RESEARCH TRIANGLE PARK, NC 27709-2211	1
DIRECTOR U.S. NAVAL RESEARCH LABORATORY ATTN: MATERIALS SCI & TECH DIV WASHINGTON, D.C. 20375	1
WRIGHT LABORATORY ARMAMENT DIRECTORATE ATTN: WL/MNM EGLIN AFB, FL 32542-6810	1
WRIGHT LABORATORY ARMAMENT DIRECTORATE ATTN: WL/MNMF EGLIN AFB, FL 32542-6810	1

NOTE: PLEASE NOTIFY COMMANDER, ARMAMENT RESEARCH, DEVELOPMENT, AND ENGINEERING CENTER, BENÉT LABORATORIES, CCAC, U.S. ARMY TANK-AUTOMOTIVE AND ARMAMENTS COMMAND, AMSTA-AR-CCB-O, WATERVLIET, NY 12189-4050 OF ADDRESS CHANGES.